Exp.-Nr. **A2**
Eingang:
an PAC:

Mainz Microtron MAMI

A2 Collaboration at MAMI
Spokespersons: P. Pedroni, A. Thomas

Proposal for an Experiment

"C-symmetry violating ($\pi^0 \to 3\gamma$)"

Spokespersons for the Experiment :
Cristina Collicott (Johannes Gutenberg Universitaet/George Washington University)
Wolfgang Gradl (Johannes Gutenberg Universitaet, Mainz, Germany)

Abstract of Physics :
We propose a search for evidence of the C-symmetry violating ($\pi^0 \to 3\gamma$) decay. An observation of this decay channel would be the first experimental confirmation of the C-symmetry violating decay of π^0 mesons. Additionally, because the interaction proceeds via the electromagnetic force, an observation of this channel would be the first evidence of C-symmetry violation in the electromagnetic interactions. Additionally, if possible, we would aim to set a new upper bound for the rare decay of ($\pi^0 \to 4\gamma$).

Abstract of Equipment :
The experiment will be performed at the tagged photon facility of MAMI using the upgraded focal plane detector, along with a portion of untagged beamtime. Event detection will be accomplished with the Crystal Ball/TAPS detector setup, along with the particle identification detectors (PID II and PID III).

MAMI Specifications :

beam energy	250 MeV
beam polarization	unpolarized

Photon Beam Specifications :

tagged energy range	Un-tagged
photon beam polarization	unpolarized

Equipment Specifications :

detectors	Crystal Ball/TAPS, PID II and PID III
target	^{16}O / ^{40}Ca

Beam Time Request :

set-up/test with beam	50 hours
data taking	300 hours

List of participating authors:

- **Institut für Physik, University of Basel, Switzerland**
  S. Abt, S. Garni, M. Günther, A. Käser, B. Krusche, S. Lutterer, M. Oberle, Th. Strub, N.K. Walford, L. Witthauer
- **Institut für Experimentalphysik, University of Bochum, Germany**
  G. Reicherz
- **Helmholtz–Institut für Strahlen- und Kernphysik, University of Bonn, Germany**
  F. Afzal, R. Beck, K. Spieker, A. Thiel
- **JINR, Dubna, Russia**
  N.S. Borisov, A. Lazarev, A. Neganov, Yu.A. Usov
- **SUPA School of Physics, University of Edinburgh, UK**
  M. Bashkanov, S. Kay, D.P. Watts, L. Zana
- **SUPA School of Physics and Astronomy, University of Glasgow, UK**
  J.R.M. Annand, D. Hamilton, D.I. Glazier, S. Gardner, K. Livingston, R.Macrae , I.J.D. MacGregor, C. Mullen, D. Werthmüller
- **Department of Astronomy and Physics, Saint Mary's University Halifax, Canada**
  A.J. Sarty
- **Racah Institute of Physics, Hebrew University of Jerusalem, Israel**
  G. Ron
- **Kent State University, Kent, USA**
  C.S. Akondi, D.M. Manley
- **Institut für Kernphysik, University of Mainz, Germany**
  P. Achenbach, H.J. Arends, M. Biroth, F. Cividini, A. Denig, P. Drexler, M.I. Ferretti-Bondy, W. Gradl, V.L Kashevarov, P.P. Martel, A. Neiser, E. Mornacchi, M. Ostrick, S.N. Prakhov, V. Sokhoyan, C. Sfienti, O. Steffen, M. Thiel, A. Thomas, S. Wagner, J. Wettig, M. Wolfes
- **University of Massachusetts, Amherst, USA**
  R.Miskimen, A. Rajabi
- **Institute for Nuclear Research, Moscow, Russia**
  G. Gurevic, R. Kondratiev, V. Lisin, A. Polonski
- **INFN Sezione di Pavia, Pavia, Italy**
  A. Braghieri, S. Costanza, P. Pedroni
- **Department of Physics, University of Regina, Canada**
  Z. Ahmed, G.M. Huber, D. Paudyal
- **Mount Allison University, Sackville, Canada**
  D. Hornidge
- **Tomsk Polytechnic University, Tomsk, Russia**
  A. Fix

- **George Washington University, Washington, USA**
  W.J. Briscoe, C. Collicott, E.J. Downie, I.I. Strakovski
- **Rudjer Boskovic Institute, Zagreb, Croatia**
  M. Korolija, I. Supek

1 Motivation

The study of C- and CP-symmetry violation aims to answer a fundamental question of physics: are matter and anti-matter subject to the same laws of physics? Clues from astrophysics, primarily the preference for matter over anti-matter in the Universe, would suggest that matter and anti-matter may in fact be intrinsically different. If the very early Universe began with no asymmetry between matter and anti-matter, then it must be that the physics which governs their interactions created a preference for matter within our Universe. The leading theory, Baryogenesis, requires both C- and CP-symmetry violation. Studies of symmetry violation provide an interesting opportunity to understand the physics governing the largest scales of the Universe within experimental physics facilities.

Charge conjugation, characterized by the C-operator, transforms a particle into it's antiparticle in the same state. C-symmetry is often discussed along with two other basic symmetries: parity (P) symmetry and time-reversal (T) symmetry. Parity, characterized by the P-operator, transforms the spatial coordinates of a particle, flipping the coordinate system such that $(x, y, z) \rightarrow (-x, -y, -z)$. Time-reversal, characterized by the T-operator, transforms the temporal coordinates of a particle, flipping the coordinate system such that $(t) \rightarrow (-t)$. Each operator has the property that when applied twice, the system is returned to the original state. This can be summarised as $C^2 = P^2 = T^2 = 1$. Together, these basic symmetries can be thought to effect the particle (C), space (P), and time (T). It is also interesting to note that these basic symmetries can be combined to form additional symmetries. CP-symmetry, for example, combines C-symmetry and P-symmetry. When both C and P are applied to a particle, we obtain a mirror image of the antiparticle.

The ways in which individual particles, or forces, violate or obey symmetries is an interesting physics probe. Strong and electromagnetic interactions observe C- and P-symmetry, and therefore must also observe CP symmetry. However, this is not true for interactions governed by the weak force. The violation of P-symmetry in weak interactions was first demonstrated by Chien-Shiung Wu in 1957 through the study of the β decay of ^{60}Co to ^{60}Ni [1]. Lee and Yang, the theorists involved in the Wu experiment, were awarded the Nobel prize in physics in 1957. With the developments of Wu, it was clear that interactions governed by the weak force were not required to observe C- or P-symmetry. At the time, it was still believed that CP-symmetry would apply. However, evidence of CP-symmetry violation was observed by Christenson *et.al.* in 1964 while studying the decays of neutral kaon, K^0, mesons [2]. This discovery was awarded the Nobel Prize in physics in 1980. In the years since this discovery, further C-, P-, and CP-symmetry violating interactions have been studied, and it is now clear that interactions governed by the weak force do not observe these symmetries. The Standard Model, as it was in 1964, could not explain these symmetry violating decays. It was not until 1973, when Kobayashi and Maskawa proposed the existence of a third family of quarks (extending the total number of quarks to six), that the Standard Model could account for CP violating decays [3]. The existence of these additional quarks would later be confirmed by experiment and Kobayashi and Maskawa were awarded the Nobel Prize in physics in 2008. Despite the simplicity of the Kobayashi-Maskawa (KM) mechanism, it has successfully explained all CP-violation experiments to date. However, the KM mechanism fails to account completely for the observed matter/anti-matter asymmetry. This mechanism predicts an asymmetry several orders of magnitude smaller than that observed in our Universe. This

discrepancy leads to the conclusion that the Kobayashi-Maskawa mechanism alone cannot be responsible for the level of CP violation observed in the Universe. This suggests that the Standard Model is incomplete.

Experiments aimed at studying symmetry violation can provide the key to understanding the physics which governs matter and anti-matter. Experimentally, one can search for symmetry violating decays, comparing experimental results to predictions from the Standard Model, and look for discrepancies. Thus, each experimental result becomes a piece of a larger puzzle. When we discover puzzle pieces which do not fit together (discrepancies in measurements), we are probing new physics beyond the Standard Model. In this way, the study of symmetry violating decays provides a very powerful and sensitive test for finding new physics beyond the Standard Model.

2 Proposed Research

It is proposed to study the rare decay of a π^0 meson into 3 photons ($\pi^0 \to 3\gamma$). This decay tests C-symmetry violation. π^0-mesons are neutral mesons comprised of either $u\bar{u}$ or $d\bar{d}$ quarks. The dominant decay channels are [4]:

$$\pi^0 \to 2\gamma \quad : \quad \text{Branching ratio, } \Gamma = 98.823 \pm 0.034\% \tag{1}$$

$$\pi^0 \to e^+e^-\gamma \quad : \quad \text{Branching ratio, } \Gamma = \ 1.174 \pm 0.035\% \tag{2}$$

By comparison to the $\pi^0 \to 2\gamma$ decay, the decay of $\pi^0 \to 3\gamma$ can be considered extremely rare. The Standard Model prediction for the ratio of the two branching ratios is given by [5],

$$\frac{\Gamma(\pi^0 \to 3\gamma)_{\text{SM}}}{\Gamma(\pi^0 \to 2\gamma)_{\text{SM}}} = 10^{-31}. \tag{3}$$

Meson	Mass [MeV/c^2]	J^{PC}	Lifetime, τ [s]	cτ [m]
π^0	135	0^{-+}	8.5×10^{-17}	2.5×10^{-8}
π^+ / π^-	140	0^-	2.6×10^{-8}	7.8
η	548	0^{-+}	5.0×10^{-19}	1.5×10^{-10}
ω	783	1^{--}	7.8×10^{-23}	2.3×10^{-14}
η'	958	0^{-+}	3.3×10^{-21}	9.9×10^{-13}

Table 1: Subset of pseudoscalar and vector mesons with masses below 1 GeV. [4]

The π^0 has a charge conjugation value $C_{\pi^0} = +1$ (see Table 1). A photon, γ, has a charge conjugation value C_γ = -1. When considering a system of n photons, the charge conjugation value of the system is simply given by $C_{n\gamma} = (-1)^n$. It is plain to see that the dominant decay channel of the π^0 meson into 2 photons ($\pi^0 \to 2\gamma$) easily conserves C-symmetry with $C_{\pi^0} = C_{\gamma\gamma} = +1$. However, the decay of a π^0 into 3 photons (or any state with an odd number of photons) will directly violate C conservation as the decay requires a transition from C of +1 to -1. The best experimental upper bound for this decay is provided by experiments using the Crystal Box detector at Los Alamos. In their

analysis, neutral pions were produced via the interaction ($\pi^- + p \rightarrow \pi^0 + n$). This analysis provided the current best upper limit [6],

$$\frac{\Gamma(\pi^0 \rightarrow 3\gamma)_{\text{Crystal Box}}}{\Gamma(\pi^0 \rightarrow 2\gamma)_{\text{Crystal Box}}} < 3.1 \times 10^{-8}. \tag{4}$$

This research proposes a new experiment, with the A2 collaboration to study this C non-invariant decay of a π^0 meson into 3 photons ($\pi^0 \rightarrow 3\gamma$) with a factor of $100\times$ greater sensitivity than previously accomplished by the Crystal Box collaboration. It is also worth noting that such an experiment could also be sensitive to the rare decay 4γ decay of a π^0 meson. A bi-product of this analysis could be an improvement of the current upper limit for the branching ratio of the 4γ decay, with the leading upper bound provided by the Los Alamos Crystal Box experiment [6],

$$\frac{\Gamma(\pi^0 \rightarrow 4\gamma)_{\text{Crystal Box}}}{\Gamma(\pi^0 \rightarrow 2\gamma)_{\text{Crystal Box}}} < 2.8 \times 10^{-8}. \tag{5}$$

This experiment would maximize the photoproduction of π^0 mesons, with a specific effort to maximize the readout of ($\pi^0 \rightarrow 3\gamma$) events. This experiment would use a photon beam incident upon a target (such as ^{40}Ca or ^{16}O) to increase rates. Both the dominant decays ($\pi^0 \rightarrow 2\gamma$ and $\pi^0 \rightarrow e^+e^-\gamma$) could pose challenging backgrounds, however in each case, there are techniques which can be applied. Due to the dominance of these background channels, it is necessary to reject these events at the trigger level (with additional rejection in offline analyses). A discussion of trigger suppression is presented in section 4. It is proposed to run with an incident electron energy of approximately 250 MeV. It is not beneficial to move to higher energies as the increase in π^0 photoproduction is relatively small, but the increase in background channels (especially those coming from $2\pi^0$ photoproduction) adds additional complications. In addition to the main beam time, short beam time to investigate the ideal running conditions is requested (see Section 5).

An observation of this decay channel would be the first experimental confirmation of the C-symmetry violating decay of π^0 mesons. Additionally, because the interaction proceeds via the electromagnetic force, an observation of this channel would be the first evidence of C-symmetry violation in the electromagnetic interactions. To date, it is believed that the strong interaction, electromagnetism, and gravity obey C-symmetry, while it is known that interactions governed by the weak force may violate C-symmetry. An observation of C-symmetry violation in the electromagnetic force would push the Standard Model into the regime of new physics.

3 Experimental setup

This experiment is proposed to run with the A2 collaboration at MAMI. A full description of the standard experimental apparatus for the A2 collaboration is outlined in Appendix A. The following section outlines only the developments and improvements to the standard apparatus which are planned.

3.1 Upgraded Tagger Focal Plane

A new development project is planned for the A2 collaboration to improve the tagger focal plane detector. As discussed in Appendix A.1, a photon beam is produced from accelerated MAMI electrons via a Bremsstrahlung process. The energy of the photon is inferred through the process of tagging the retarded electron. For an incident electron with initial state (E_o) and final state (E), with a produced Bremsstrahlung photon (k), energy conservation requires,

$$k = E_o - E. \tag{6}$$

As the incident electron energy is known very accurately and precisely, by measuring the retarded electron energy the photon energy is known. The Glasgow Tagged Photon Spectrometer, or Tagger, uses a large dipole magnet to bend the path of the electron. The radius of curvature of a charged particle within a magnetic field is given by,

$$r = \frac{p}{qB}. \tag{7}$$

For a given magnetic field, B, the radius of curvature will depend directly on the momentum, p, of the particle. Thus, the position along the focal plane detector can be used to determine the energy of the bremsstrahlung electron. The magnetic field strength, B, is chosen such that electrons which did not interact within the radiator are bent into a beam dump.

Currently, the tagger focal plane detector (FPD) comprises 353 plastic scintillators. Each scintillator is roughly (2 cm $\times$ 2 mm $\times$ 8 cm) and is coupled to a photomultiplier tube, PMT. Additionally, each scintillator overlaps with the neighbouring scintillators by roughly 50%. To identify electron signals, a "hit" is formed in the FPD when there is a coincidence between two overlapping scintillators. The requirement of a coincidence between two scintillators results in 352 tagger channels. The existing FPD has a maximum electron rate of 10^6 electrons per channel. As the magnetic field is set differently for each incident photon energy, the maximum rate of electrons per MeV is different. An example of this is given in Table 2. A plan to upgrade the existing focal plane is currently underway. This upgrade will replace the existing focal plane detector with set of small scintillators, each measuring (6 mm $\times$ 6 mm $\times$ 30 mm). Additional studies are ongoing which would use scintillators measuring (3 mm $\times$ 3 mm $\times$ 30 mm). Readout is accomplished using silicon photomultipliers, SiPMs, along with new electronics. An increase in the maximum electron rate ($\times$2.5) is accomplished with the new readout. An additional increase in the maximum electron rate ($\times$2) is accomplished by removing the scintillator overlaps which existed in the orignal FPD design. Together, this gives a maximum electron rate of 5×10^6 electrons per channel.

	200 MeV	450 MeV	880 MeV	1600 MeV
Current Focal Plane limitations				
Maximum electron rate/per tagger ch..	10^6	10^6	10^6	10^6
Maximum electron rate/per MeV	2×10^6	10^6	0.5×10^6	0.25×10^6
Upgraded Focal Plane limitations				
Maximum electron rate/per tagger ch.	$5{\times}10^6$	$5{\times}10^6$	$5{\times}10^6$	$5{\times}10^6$
Maximum electron rate/per MeV	10^7	5×10^6	2.5×10^6	1.25×10^6

Table 2: Electron rate (s^{-1}) limitations for the current and upgraded focal plane detectors.

3.2 PID III

As discussed in Appendix A.3, identification of charged particle species in the Crystal Ball system is accomplished with the Particle Identification Detector (PID). The existing PID, known as PID II, comprises 24 plastic scintillators (4 mm thick) arranged in a barrel surrounding the target. Each scintillator element subtends an angle of 15° in ϕ. Recently (August 2016), a new PID detector (PID III) was constructed. While the design of PID III is nearly identical to PID II (as shown in Table 3), the inner radius of PID III is smaller. This key difference allows for the possibility to combine PID II and PID III within the same experimental setup. In this case, the two detectors would sit coaxial to the target and beamline. They could also be rotated slightly relative to each other to provide improved segmentation of the azimuthal angle (7.5 °) when the overlap of scintillators is considered. This approach, would also improve the detection efficiency of charged particles by providing overlapping scintillator coverage.

	PID II	**PID III**
No. of Scintillators	24	24
Scintillator material	EJ-204	EJ-204
Scintillator thickness [mm]	4	4
Scintillator length [mm]	50	30
Inner Radius [cm]	5.8	3.3 cm
Polar (θ) angular coverage	21° - 159°	21° - 159°
Azimuthal (ϕ) angular coverage	0° - 180° (15° steps)	0° - 180° (15° steps)

Table 3: Similarities and differences between the two particle identification detectors, PID II and PID III.

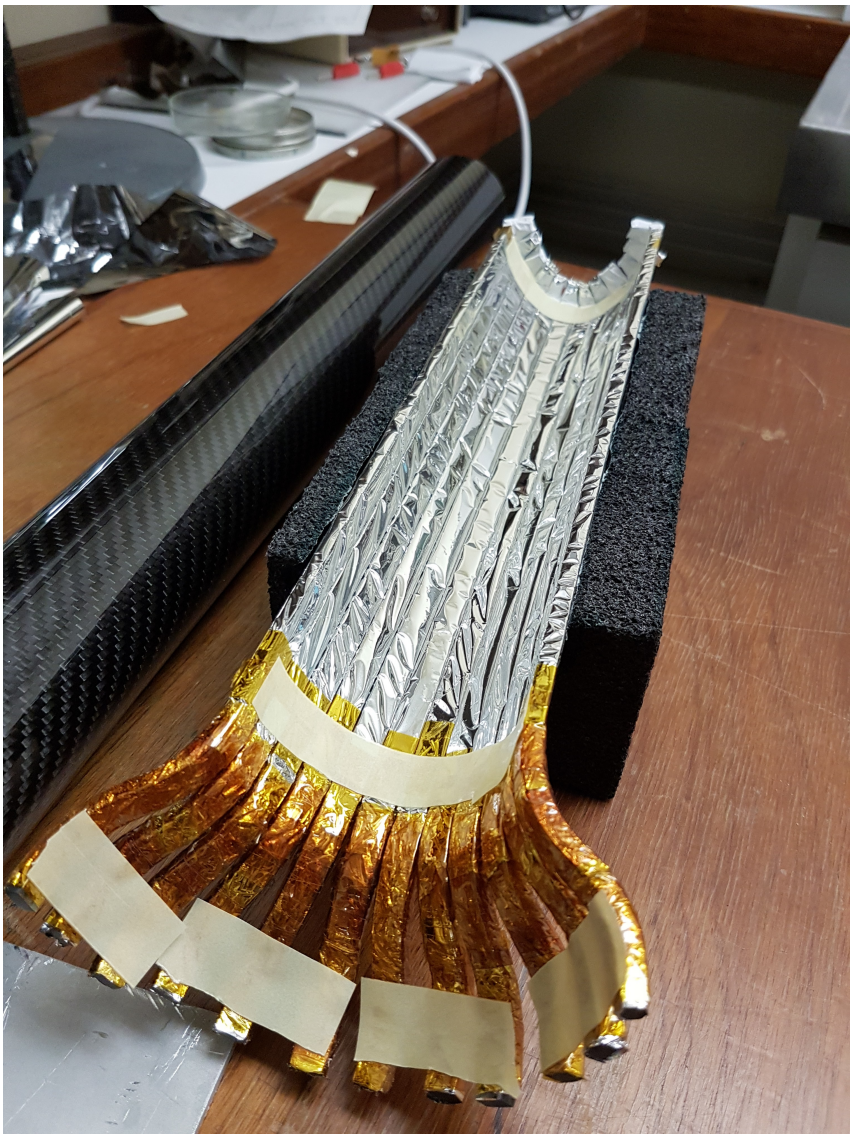

Figure 1: Construction of PID III: half of the scintillator elements are shown.

3.3 Targets: ^{40}Ca and ^{16}O

Previous experiments [7] [8] in the A2 experimental hall have been performed involving ^{40}Ca and ^{16}O targets. In Ref. [7] coherent photoproduction cross sections were measured for a variety of targets. As discussed within this reference, when working with a ^{40}Ca target, the target should sit within a vacuum to help prevent oxidation. A simple vacuum pipe was constructed from Carbon Fiber and ROHACELL foam. For ^{16}O, a water target was used, and a schematic is shown in Figure 2. Assuming that PID II and PID III are used together (see Section 3.2), the radius of the target and target pipe must fit within the inner radius of PID III (3.2 cm). The physical properties of the ^{40}Ca target discussed in Ref. [7] are presented in Table 4.

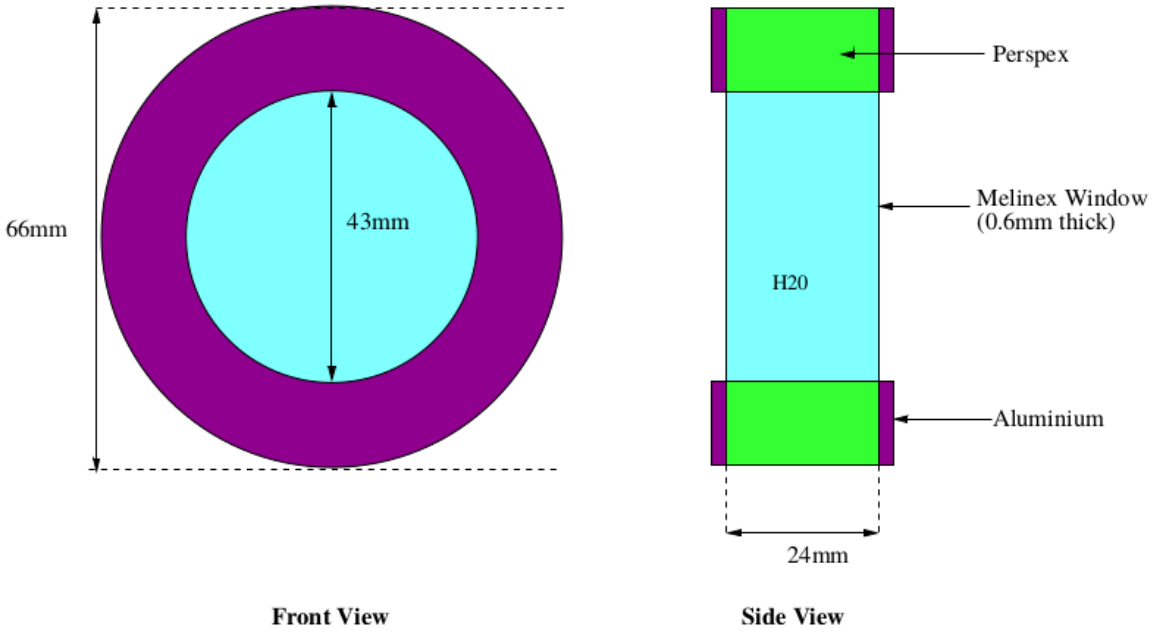

Figure 2: Schematic of water target (^{16}O) used in Ref. [7].

	^{40}**Ca target**	^{16}**O target**
Dimensions (radius) [mm]	21	43
Dimensions (thickness) [mm]	10 ± 0.5	31.4 ± 0.5
Purity (natural Calcium)	97 %	99.75 %
Density [nuclei/cm^2]	3.0×10^{22}	6.6×10^{22}

Table 4: Proposed ^{40}Ca and ^{16}O target parameters.

In the following section, a series of simulations for the ^{40}Ca target are presented. Simulations for the ^{16}O are ongoing.

4 Backgrounds and Trigger Conditions

As discussed in Section 2, it is intended to measure the rare, C-symmetry violating decay of a π^0 meson into 3 photons. Considering equations 1, 2, and 4, we can can compare the relative branching ratios of π^0 decays:

$$\begin{aligned} \pi^0 \to 2\gamma &: \quad \text{Branching ratio, } \Gamma_{2\gamma} = 98.823 \pm 0.034\ \% \\ \pi^0 \to e^+e^-\gamma &: \quad \text{Branching ratio, } \Gamma/\Gamma_{2\gamma} = 1.2 \times 10^{-2}\ \% \\ \pi^0 \to \gamma\gamma\gamma &: \quad \text{Branching ratio, } \Gamma/\Gamma_{2\gamma} < 3.1 \times 10^{-8}\ \% \end{aligned}$$

It is intended to produce a data set of π^0 mesons via photoproduction; this production can proceed by a variety of channels. These channels include the coherent photoproduction process, incoherent processes (with the nucleus left in an excited state), quasifree processes (with the knock-out of a nucleon), and double π^0 production. For ^{40}Ca, the coherent photoproduction channel is,

$$\gamma + {}^{40}\text{Ca} \to \pi^0 + {}^{40}\text{Ca} \tag{8}$$

For the incoherent/quasi-free processes to proceed, additional energy is involved. For nuclear excitation, this energy corresponds to the energy shift associated with the nuclear energy levels. For quasi-free this energy corresponds to the required energy to overcome the knockout energy of the nucleon. Finally, for double π^0 production, this energy corresponds to the mass of the second π^0 meson. By staying below the threshold of double π^0 production, we can ignore this process.

	Reaction ($\gamma + {}^{40}\text{Ca} \to \cdots$)	Energy [MeV]
Nuclear Excitation	$\pi^0 + {}^{40}\text{Ca}^*$	3.7, 4.5, 6.9 $\cdots$
Quasi-free (proton knockout)	$\pi^0 + p + {}^{39}\text{K}$	12.5
Quasi-free (neutron knockout)	$\pi^0 + n + {}^{39}\text{Ca}$	9.9
Double π^0 production	$\pi^0 + \pi^0 + {}^{40}\text{Ca}$	134.98

Table 5: Summary of the energy required (beyond coherent photoproduction) for incoherent photoproduction processes involving π^0 mesons and a ^{40}Ca nucleus. [7]

As the upper limit for the $\pi^0 \to 3\gamma$ decay ($\Gamma/\Gamma_{2\gamma}$) is of the order 10^{-8}, it is clear that control of background channels is both challenging and necessary. While separation of the channels is necessary at the analysis stage, some suppression of the background channels will also necessary at the trigger level. The following sections will outline what level of background suppression is **possible**. It will be discussed in Section 5 what level of background suppression is **necessary**.

4.1 Background suppression: coherent processes

The following outlines an investigation of background suppression for coherent processes, produced according to equation 8. The following decays are considered:

$$\pi^0 + {}^{40}\text{Ca} \to {}^{40}\text{Ca} + \gamma\gamma\gamma \tag{9}$$

$$\pi^0 + {}^{40}\text{Ca} \to {}^{40}\text{Ca} + \gamma\gamma \tag{10}$$

$$\pi^0 + {}^{40}\text{Ca} \to {}^{40}\text{Ca} + e^+e^-\gamma \tag{11}$$

Background suppression at the trigger level is limited to relatively simple concepts. For these reactions, there are four trigger cuts which are of particular interest: (1) multiplicity, (2) neutrality, (3) minimum cluster energy, and (4) minimum opening angle.

The Crystal Ball and TAPS are both highly segmented detectors. As particles pass through the detector system, they typically deposit their energy via electromagnetic showers. This deposition by EM shower means that the particle's energy will be distributed over many individual detector elements, or crystals. These crystals can then be reconstructed to form clusters. The **multiplicity**, M, of an event is defined simply as the number of clusters reconstructed during that event. A naive prediction for the multiplicity of the reactions outlined in equations 9, 10, and 11 would be M = 3, 2, and 3 respectively. We would, of course, expect a multiplicity of 2 for the $\pi^0 \to 2\gamma$ case. However, in reality this is often more complicated. Although the Crystal Ball and TAPS detector systems cover most of the 4π solid angle, it is possible for one decay photon to go undetected. It is also possible for one of the decay photons to be falsely detected as two clusters. This is known as a *split-off* cluster. In Figure 3, a simulated multiplicity distribution is shown for the processes outlined in equations 9 and 10. While the $\pi^0 \to 2\gamma$ decay case clearly peaks at M=2, a small portion of the events will have M=3. Because of the overwhelming dominance of the 2γ case, this presents a significant background.

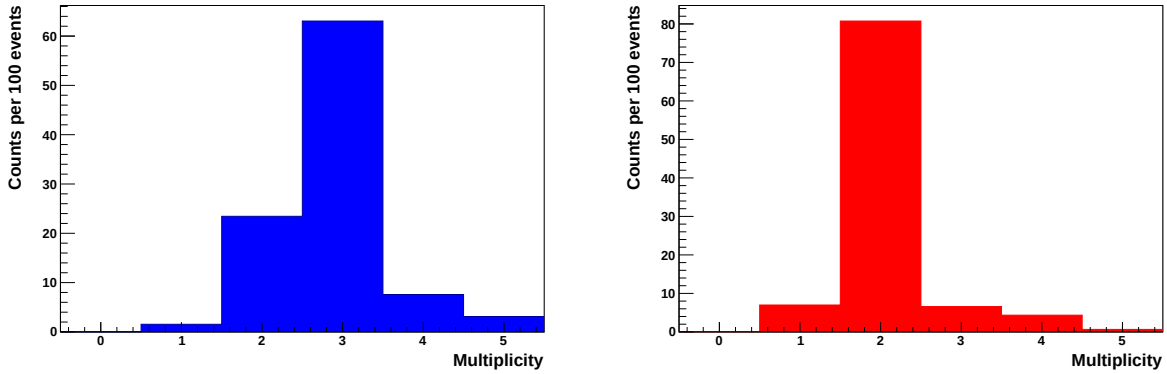

(a) $\pi^0 + {}^{40}\text{Ca} \to {}^{40}\text{Ca} + \gamma\gamma\gamma$ (b) $\pi^0 + {}^{40}\text{Ca} \to {}^{40}\text{Ca} + \gamma\gamma$

Figure 3: Simulated multiplicities for coherent π^0 photoproduction (γ-energy = 165 MeV) showing a comparison of the reaction channel ($\pi^0 \to \gamma\gamma\gamma$) to the background channel ($\pi^0 \to \gamma\gamma$).

The Crystal Ball and TAPS are both equipped with charged particle detectors, see Appendix A.3 and Section 3.2 for a complete discussion. The **neutrality**, N, of the event is defined by the presence of any signal within the charged particle detectors. If any signal is present in the PID or TAPS Veto wall (which implies a charged particle is involved), the neutrality test fails and the event has N=0. Otherwise, the event passes the neutrality test and N=1. A naive prediction for the neutrality of the reactions outlined in equations 9, 10, and 11 would be N = 1, 1, and 0 respectively. In Figure 4, a simulated neutrality distribution is shown for the processes outlined in equations 9 and 11. At present, only PID II is included in the simulations, however the inclusion of PID III will further suppress the charged $\pi^0 \to e^+e^-\gamma$ background.

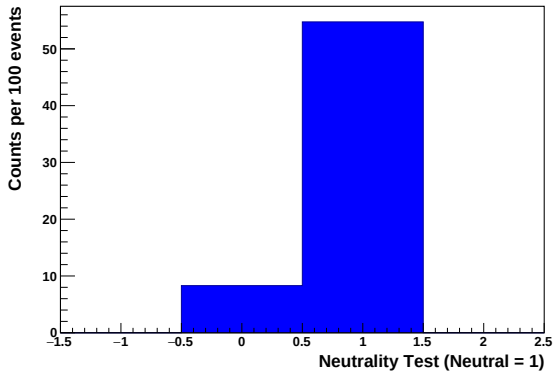

(a) $\pi^0 + ^{40}\text{Ca} \rightarrow ^{40}\text{Ca} + \gamma\gamma\gamma$

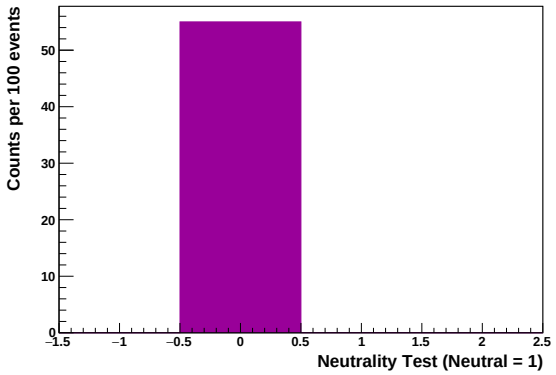

(b) $\pi^0 + ^{40}\text{Ca} \rightarrow ^{40}\text{Ca} + e^+e^-\gamma$

Figure 4: Simulated acceptance based upon a neutrality test for coherent π^0 photoproduction (γ-energy = 165 MeV) showing a comparison of the reaction channel ($\pi^0 \rightarrow \gamma\gamma\gamma$) to the charged background channel ($\pi^0 \rightarrow e^+e^-\gamma$). A test value of N = 1 corresponds to events which were determined to be neutral (ie. all clusters had no charged particle detector signals). The multiplicity requirement M=3 has been applied.

The third trigger condition which is useful for background suppression is a cut on the **minimum cluster energy**, CE. This cut simply asks that the energy of all three clusters (established by the multiplicity cut) is above a minimum value. This cut is particularly helpful to suppress the $\pi^0 \rightarrow 2\gamma$ decay where the third cluster, the split-off cluster, is typically low energy. Figure 5 shows the lowest cluster energy for the reactions outlined in equations 9, 10, and 11. The upper limit for the minimum cluster energy occurs when the π^0 energy is shared equally among the decay particles. Assuming an incident photon energy of γ-energy = 165 MeV, and M=3, the upper limit on the minimum cluster energy is roughly 55 MeV.

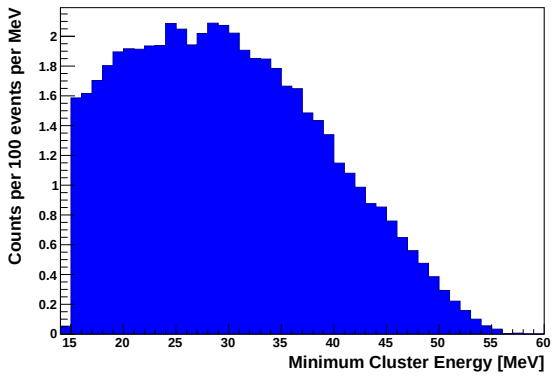

(a) $\pi^0 + ^{40}\text{Ca} \rightarrow ^{40}\text{Ca} + \gamma\gamma\gamma$

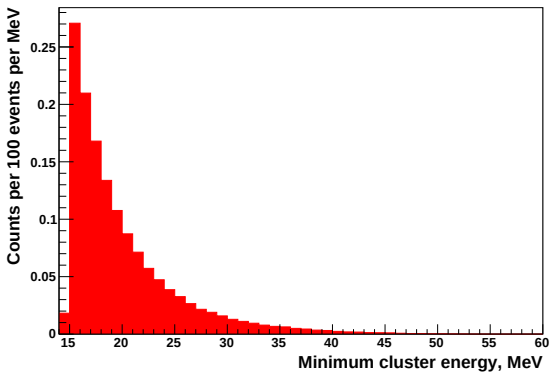

(b) $\pi^0 + ^{40}\text{Ca} \rightarrow ^{40}\text{Ca} + \gamma\gamma$

Figure 5: Simulated minimum cluster energy, CE, for coherent π^0 photoproduction (γ-energy = 165 MeV) showing a comparison of the reaction channel ($\pi^0 \rightarrow \gamma\gamma\gamma$) to the background channel ($\pi^0 \rightarrow \gamma\gamma$).

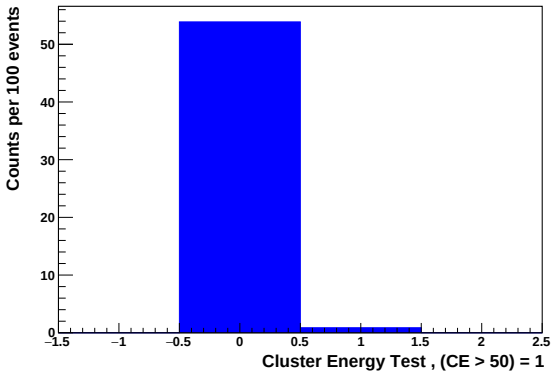

(a) $\pi^0 + {}^{40}\text{Ca} \rightarrow {}^{40}\text{Ca} + \gamma\gamma\gamma$

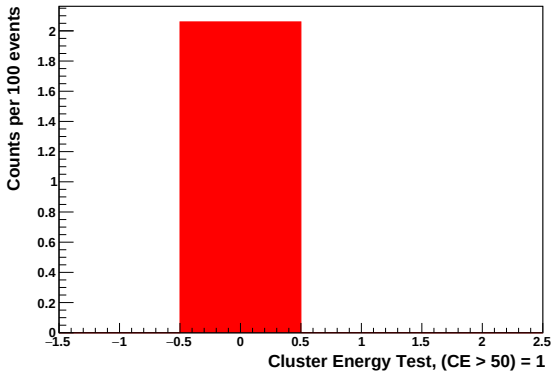

(b) $\pi^0 + {}^{40}\text{Ca} \rightarrow {}^{40}\text{Ca} + \gamma\gamma$

Figure 6: Simulated acceptance based upon a minimum cluster energy, CE $>$ 50 MeV, test for coherent π^0 photoproduction (γ-energy = 165 MeV) showing a comparison of the reaction channel ($\pi^0 \rightarrow \gamma\gamma\gamma$) to the background channel ($\pi^0 \rightarrow \gamma\gamma$). While both reactions experience strong suppression, the background channel is more strongly suppressed. The multiplicity requirement, M=3, and neutrality requirement, N=1, have been applied.

The fourth trigger condition of interest is the **minimum opening angle**, OA. For any two vectors, $\vec{p}_{\text{A}}$ and $\vec{p}_{\text{B}}$, the angle between the vectors, Ω_{OA}, is defined by,

$$\cos(\Omega_{\text{OA}}) = \frac{\vec{p}_{\text{A}} \cdot \vec{p}_{\text{B}}}{|\vec{p}_{\text{A}}| \times |\vec{p}_{\text{B}}|} \, . \tag{12}$$

This opening angle is essentially the 2-dimensional (θ and ϕ) angle between two clusters. This cut simply asks that each opening angle between all three clusters (established by the multiplicity cut) is above a minimum value. This cut is particularly helpful to suppress the $\pi^0 \rightarrow 2\gamma$ decay where the third cluster, the split-off cluster, is typically close to the primary cluster. While this trigger condition is relatively difficult to create, a very similar trigger condition was accomplished in 2012 to require coplanarity of clusters. This coplanarity trigger was accomplished by creating a look up table corresponding to the allowed cluster groups. The trigger was tested with real data in December 2012 and behaved as expected. The same approach, involving a look up table, could be applied to create the minimum opening angle trigger condition .

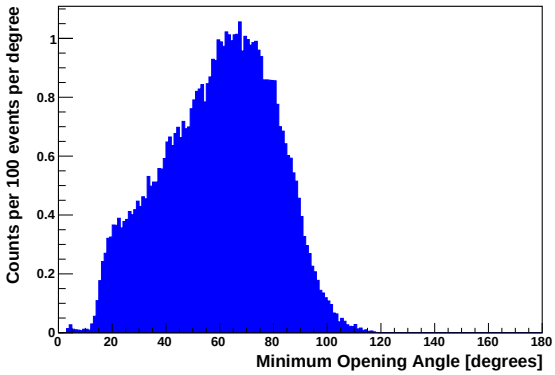

(a) $\pi^0 + ^{40}\text{Ca} \rightarrow ^{40}\text{Ca} + \gamma\gamma\gamma$

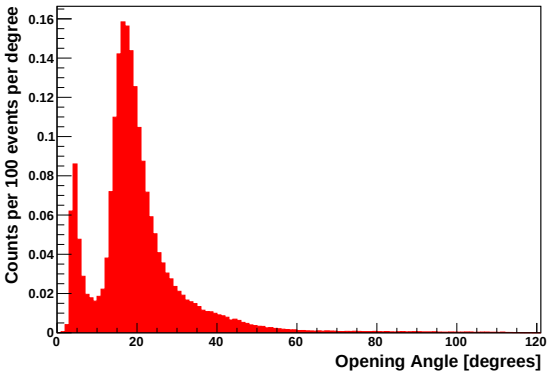

(b) $\pi^0 + ^{40}\text{Ca} \rightarrow ^{40}\text{Ca} + \gamma\gamma$

Figure 7: Simulated minimum opening angle, OA, for coherent π^0 photoproduction (γ-energy = 165 MeV) showing a comparison of the reaction channel ($\pi^0 \rightarrow \gamma\gamma\gamma$) to the background channel ($\pi^0 \rightarrow \gamma\gamma$).

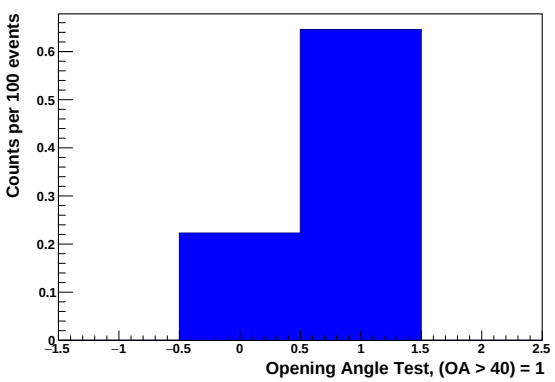

(a) $\pi^0 + ^{40}\text{Ca} \rightarrow ^{40}\text{Ca} + \gamma\gamma\gamma$

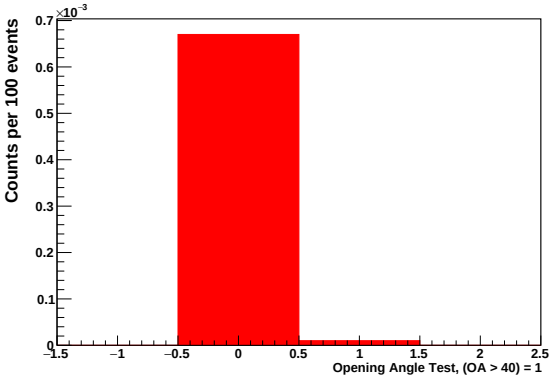

(b) $\pi^0 + ^{40}\text{Ca} \rightarrow ^{40}\text{Ca} + \gamma\gamma$

Figure 8: Simulated acceptance based upon a minimum opening angle, OA $> 40°$, test for coherent π^0 photoproduction (γ-energy = 165 MeV) showing a comparison of the reaction channel ($\pi^0 \rightarrow \gamma\gamma\gamma$) to the background channel ($\pi^0 \rightarrow \gamma\gamma$). The multiplicity requirement, M=3, neutrality requirement, N=1, and cluster energy, CE > 50 MeV have been applied.

The trigger conditions outlined in Table 6 do an excellent job of suppressing the unwanted backgrounds, however the low detection efficiency of the $\pi^0 \rightarrow 3\gamma$ channel makes it interesting to loosen the trigger conditions. Shown in Table 7 are the trigger acceptance rates for a cluster energy cut of 45 MeV rather than 50 MeV.

Trigger Condition	$\pi^0 \to 3\gamma$	$\pi^0 \to 2\gamma$	$\pi^0 \to e^+e^-\gamma$
Multiplicity, M=3	63 %	6.5 %	55 %
+ Neutrality, N=1	55 %	2 %	10^{-2} %
+ Cluster Energy, CE > 50 MeV	0.9 %	7×10^{-4} %	< 1 in 10^{-8}
+ Opening Angle, OA > 40 °	0.7 %	10^{-5} %	< 1 in 10^{-8}

Table 6: Summary of the simulated trigger acceptance rates for coherent π^0 photoproduction (γ-energy = 165 MeV). Four trigger conditions are proposed based on the multiplicity, neutrality, minimum cluster energy, and minimum opening angle. The rates of acceptance are shown where each trigger condition is combined successively.

Trigger Condition	$\pi^0 \to 3\gamma$	$\pi^0 \to 2\gamma$	$\pi^0 \to e^+e^-\gamma$
Multiplicity, M=3	63 %	6.5 %	55 %
+ Neutrality, N=1	55 %	2 %	10^{-2} %
+ Cluster Energy, CE > 45 MeV	3.7 %	3.7×10^{-3} %	8×10^{-5} %
+ Opening Angle, OA > 40 °	2.8 %	2.5×10^{-5} %	6×10^{-5} %

Table 7: Summary of the simulated trigger acceptance rates for coherent π^0 photoproduction (γ-energy = 165 MeV). Four trigger conditions are proposed based on the multiplicity, neutrality, minimum cluster energy, and minimum opening angle. The rates of acceptance are shown where each trigger condition is combined successively.

Based on the coherent process studies, a set of possible trigger conditions which provide background rejection is as follows:

- multiplicity, M=3: three clusters,
- neutrality, N=1: all clusters neutral,
- minimum cluster energy, CE > 45 MeV: all clusters have more than 45 MeV, and
- minimum opening angle, OA > 40 °: all clusters have an angular separation greater than 40 °.

4.2 Background suppression: incoherent processes

A summary of incoherent backgrounds was presented in Table 5. As discussed previously, staying below the threshold of double π^0 production allows us to ignore this process completely. Shown below is an example of the trigger acceptance rates for quasi-free (proton knockout) process outlined in Table 5. The same trigger conditions proposed in Section 4.1 were adopted here. When the trigger condition on the minimum cluster energy is combined with the energy shifts associated with the incoherent processes, the incoherent processes are essentially suppressed.

Trigger Condition	$\pi^0 \to 3\gamma$	$\pi^0 \to 2\gamma$	$\pi^0 \to e^+e^-\gamma$
Multiplicity, M=3	65 %	6.3 %	56 %
+ Neutrality, N=1	56 %	1.7 %	2.5×10^{-2} %
+ Cluster Energy, CE > 50 MeV	2×10^{-3} %	< 1 in 10^{-8}	< 1 in 10^{-8}
+ Opening Angle, OA > 40 °	2×10^{-3} %	< 1 in 10^{-8}	< 1 in 10^{-8}

Table 8: Summary of the simulated trigger acceptance rates for quasi-free (proton knockout) π^0 photoproduction (γ-energy = 165 MeV). Four trigger conditions are proposed based on the multiplicity, neutrality, minimum cluster energy, and minimum opening angle. The rates of acceptance are shown where each trigger condition is combined successively.

Trigger Condition	$\pi^0 \to 3\gamma$	$\pi^0 \to 2\gamma$	$\pi^0 \to e^+e^-\gamma$
Multiplicity, M=3	65 %	6.3 %	56 %
+ Neutrality, N=1	56 %	1.7 %	2.5×10^{-2} %
+ Cluster Energy, CE > 45 MeV	0.45 %	< 1 in 10^{-8}	< 1 in 10^{-8}
+ Opening Angle, OA > 40 °	0.42 %	< 1 in 10^{-8}	< 1 in 10^{-8}

Table 9: Summary of the simulated trigger acceptance rates for quasi-free (proton knockout) π^0 photoproduction (γ-energy = 165 MeV). Four trigger conditions are proposed based on the multiplicity, neutrality, minimum cluster energy, and minimum opening angle. The rates of acceptance are shown where each trigger condition is combined successively.

5 Beam Time Estimate

The following presents a beamtime estimate based on the following equation:

$$N_\pi = f_\gamma \times N_t \times \sigma(\gamma + A \to \pi^0 + A) \tag{13}$$

The individual terms will be discussed in the following sections.

5.1 Estimated photon flux

The maximum photon flux is given by,

$$f_\gamma = m \times a \times \epsilon_t, \tag{14}$$

where f_γ is the photon flux rate per MeV, m is the maximum electron rate per MeV, a is the average electron rate , and ϵ_t is the tagging efficiency. It is proposed to take data at a very low incident electron energy of roughly 210 MeV. In this case the maximum electron rate (given previously in Table 2) is,

$$m = 10^7 \text{ electrons MeV}^{-1} \text{ s}^{-1} \ . \tag{15}$$

While the upgraded tagger would be employed, only a small energy region would be tagged. The proposed tagging region would include photons with energies of 150 MeV - 200 MeV. Typically the average electron rate, a, is not equal to 1 due to the shape of the bremsstrahlung distribution (where the rate of photons is roughly proportional to 1/k, the inverse of the photon energy). With such a reduced tagged photon region, the average electron rate is given by,

$$a \approx 1. \tag{16}$$

Finally, the tagging efficiency ϵ_t must be estimated from previous measurements. Table 10 outlines a selection of tagging efficiencies. As a general rule, ϵ_t is reduced as incident electron energy is reduced, and ϵ_t is reduced as collimator size is reduced. Based on the size of the ^{40}Ca target (21 mm), a collimator which is 7 mm in diameter would produce a beamspot within the target diameter. Based on this, the previously measured tagging efficiency (Nickel 4 μm, 7 mm Colli) should be a reasonable estimate of the tagging efficiency.

$$\epsilon_t = 15\% \tag{17}$$

In this case, the maximum photon flux is approximated by,

$$f_\gamma = 1.5 \times 10^6 \text{ photons MeV}^{-1} \text{ s}^{-1} \ . \tag{18}$$

	180 MeV	450 MeV	880 MeV	1600 MeV
Tagging Efficiency (Copper 10 μm, 4mm Colli)			43 %	66 %
Tagging Efficiency (Moeller, 2.5mm Colli)		8.3 %		35 %
Tagging Efficiency (Nickel 4 μm, 7mm Colli)	17 %			

Table 10: Sample of previously measured tagging efficiencies, ϵ_t

5.2 Target

The target density, given previously in Table 4, is:

$$N_t(^{40}\text{Ca}) = 3.0 \times 10^{22} \text{ nuclei cm}^{-2}, \quad N_t(^{16}\text{O}) = 6.6 \times 10^{22} \text{ nuclei cm}^{-2} \tag{19}$$

5.3 Cross section

The total coherent cross section was studied previously with the Crystal Ball detector [7]. Figure 9 shows the total cross section for incident γ energies of 140 - 260 MeV. Experimental data show a maximum cross section occuring at roughly 210 MeV for calcium and 240 MeV for oxygen.

$$\sigma(\gamma + {}^{40}\text{Ca} \rightarrow \pi^0 + {}^{40}\text{Ca})_{210MeV} = 900\ \mu\text{b} \quad (20)$$

$$\sigma(\gamma + {}^{16}\text{O} \rightarrow \pi^0 + {}^{16}\text{O})_{240MeV} = 600\ \mu\text{b} \quad (21)$$

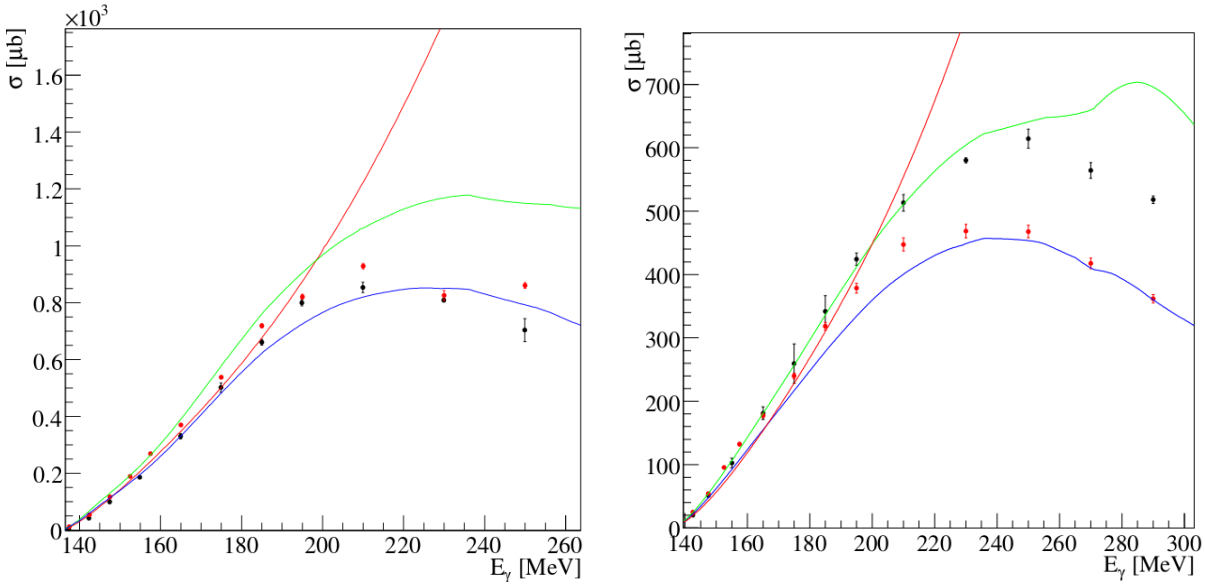

(a) ^{40}Ca (b) ^{16}O

Figure 9: Total coherent Cross section σ for ^{40}Ca and ^{16}O. Black and red points are experimental data from the Crystal Ball and TAPS detectors. The red, green, and blue curves are theoretical calculations (see original reference: [7]).

5.4 π photoproduction rate – Tagged

Applying equation 13, for ^{40}Ca we find a maximum rate of:

$$N_{\pi}\text{ rate} = \left(1.5\times10^{6}\frac{\text{photons}}{\text{MeV s}}\right)\times\left(3.0\times10^{22}\frac{\text{nuclei}}{\text{cm}^2}\right)\times\left(900\mu\text{b}\right)\times\frac{10^{-30}cm^2}{\mu\text{b}} \quad (22)$$

$$N_{\pi}\text{ rate (max.)} = 40\text{ coherent }\pi^0\text{ MeV}^{-1}\text{ s}^{-1} \quad (23)$$

Similarly for ^{16}O, we find,

$$N_{\pi}\text{ rate} = \left(1.5\times10^{6}\frac{\text{photons}}{\text{MeV s}}\right)\times\left(6.6\times10^{22}\frac{\text{nuclei}}{\text{cm}^2}\right)\times\left(600\mu\text{b}\right)\times\frac{10^{-30}cm^2}{\mu\text{b}} \quad (24)$$

$$N_{\pi}\text{ rate (max.)} = 60\text{ coherent }\pi^0\text{ MeV}^{-1}\text{ s}^{-1} \quad (25)$$

Taking the ^{16}O case (maximum rate), and assuming a tagged photon range of roughly 50 MeV, this would produce a data set **per week** of beamtime,

$$\begin{aligned} N_{\pi}(^{16}\text{O}) &= 60\text{ MeV}^{-1}\text{ s}^{-1}\times 50\text{ MeV}\times 604800\text{ s week}^{-1} \\ &= 3000\ \pi^0\text{ s}^{-1} \\ &= 1.814\times10^{9}\ \pi^0\text{ week}^{-1} \end{aligned} \quad (26)$$

Using the current upper limit as branching ratio for the $\pi^0\to3\gamma$ decay, we can determine the rate of each individual decay,

$$N_{\pi^0\to2\gamma} = 2965\text{ s}^{-1} = 1.79\times10^{9}\text{ week}^{-1} \quad (27)$$

$$N_{\pi^0\to e^+e^-\gamma} = 35\text{ s}^{-1} = 2.12\times10^{7}\text{ week}^{-1} \quad (28)$$

$$N_{\pi^0\to3\gamma} = 3\times10^{-5}\text{ s}^{-1} = 18.14\text{ week}^{-1} \quad (29)$$

At present, the DAQ rate can record approximately 3500 events s^{-1} (with a livetime of 65%). Assuming a completely open trigger, we could actually record all of these events, however, the rate of 10.25 $\pi^0\to3\gamma$ per week is not sufficient. Therefore, it is proposed to run a short test beam time which is **untagged**. In this case, the incident photon energy is unknown, but the rate is limited not by the maximum electron rate on the tagger, but rather on the maximum rate of the data acquisition system.

5.5 π photoproduction rate – Un-Tagged

Suppose we could with a photon flux $\times 5$ greater. This would be possible with increased electron beam current and/or radiator density (and is allowed since the electron rate in the Tagger Focal Plane is no longer a limiting factor).

$$N_{\pi^0 \to 2\gamma} = \quad 14825 \text{ s}^{-1} \quad = 8.95 \times 10^9 \text{ week}^{-1} \tag{30}$$

$$N_{\pi^0 \to e^+e^-\gamma} = \quad 175 \text{ s}^{-1} \quad = 1.01 \times 10^8 \text{ week}^{-1} \tag{31}$$

$$N_{\pi^0 \to 3\gamma} = \quad 1.5 \times 10^{-4} \text{ s}^{-1} \quad = 90 \text{ week}^{-1} \tag{32}$$

At this point, the rate of π^0 production exceeds the DAQ limitations. This some trigger rejection is necessary. Assuming a simple multiplicity trigger (M=3) (see Table. 6)

$$N_{\pi^0 \to 2\gamma} = \quad 963 \text{ s}^{-1} \quad = 5.8 \times 10^8 \text{ week}^{-1} \tag{33}$$

$$N_{\pi^0 \to e^+e^-\gamma} = \quad 96 \text{ s}^{-1} \quad = 5.6 \times 10^7 \text{ week}^{-1} \tag{34}$$

$$N_{\pi^0 \to 3\gamma} = \quad 9 \times 10^{-5} \text{ s}^{-1} \quad = 57 \text{ week}^{-1} \tag{35}$$

In this case, the total trigger rate would be well below the DAQ trigger rate limitation, Assuming an overall DAQ efficiency of 60%, the recorded rate of $\pi^0 \to 3\gamma$ would be ≈ 35 week^{-1}. Using these conditions, with roughly 3 weeks of beamtime, it would be possible to reduce the upper limit of the $\pi^0 \to 3\gamma$ branching ratio by ≈ 2 orders of magnitude. Also, by extending the multiplicity to include M=4, the rare $\pi^0 \to 4\gamma$ decay could be measured. This will be investigated further.

5.6 Beam-time proposal

It is not common practice for experiments in the A2 collaboration to run un-tagged. For this reason, it is proposed to take a short test beam time (2 days) to investigate the possibility of running un-tagged experiments. This short test beam time would run with a solid target, and would leave the trigger condition open enough to measure the $\pi^0 \to 2\gamma$ channel. This short beam time would be split between data with and without the Tagger focal plane detector included, where the data without the Tagger FPD will run with a maximized photon flux. This short test beam will be used to establish

- What is the maximum photon flux possible?
- At these rates, is there pile-up in the detector system from neighbouring events?
- Are the tagged/un-tagged data consistent with each other for the $\pi^0 \to 2\gamma$ channel?

Assuming the answers to these questions support continuing the experiment, the full experiment could then be scheduled. It would then be expected that 3 weeks of beamtime would be necessary to achieve a reduction of the branching ratio upper limit for the rare $\pi^0 \to 3\gamma$ decay by ≈ 2 orders of magnitude.

Appendices

A Standard Experimental apparatus in A2-MAMI

A.1 Photon Beam

The A2 photon beam is derived from the production of Bremsstrahlung photons during the passage of the MAMI electron beam through a thin radiator. The resulting photons can be circularly polarised, with the application of a polarised electron beam, or linearly polarised, in the case of a crystalline radiator. The degree of polarisation achieved is dependent on the energy of the incident photon beam (E_0) and the energy range of interest, but currently peaks at ∼75 % for linear polarisation (Fig. 10) and ∼85 % for circular polarisation (Fig. 11). In the case of linear polarisation, the degree of polarisation can be further increased with collimation. The Glasgow-Mainz Photon Tagger (Fig 12) provides energy tagging of the photons by detecting the post-radiating electrons and can determine the photon energy with a resolution of 2 to 4 MeV depending on the incident beam energy, with a single-counter time resolution $\sigma_t = 0.17$ ns [9]. Each counter can operate reliably to a rate of ~ 1 MHz, giving a photon flux of 2.5×10^5 photons per MeV. Photons can be tagged in the momentum range from 4.7 to 93.0% of E_0.

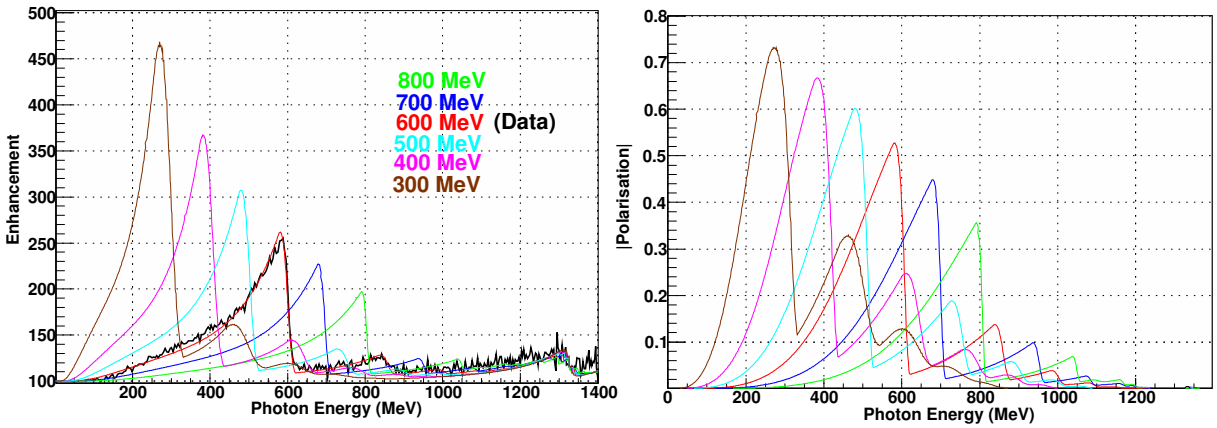

Figure 10: Linear polarisation available with the current collimation system for a variety of crystal orientations. The thin black lines are data obtained during recent MAMI-C runs.

To augment the standard focal plane detector system and make use of the Tagger's intrinsic energy resolution of 0.4 MeV (FWHM), there exists a scintillating fibre detector, known as the Tagger Microscope, that can improve the energy resolution by a factor of ∼6 for a ∼100MeV wide region of the focal plane (dependent on its position) [10].

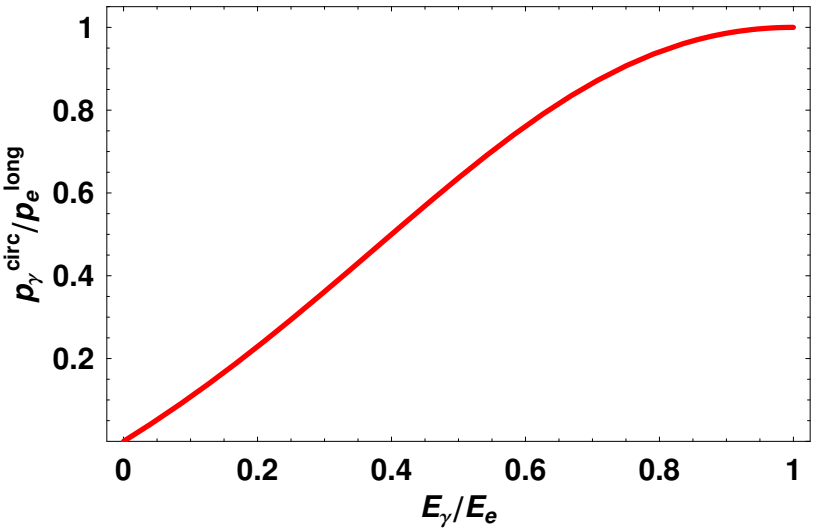

Figure 11: Helicity transfer from the electron to the photon beam as function of the energy transfer. The MAMI beam polarisation is P_e =85%.

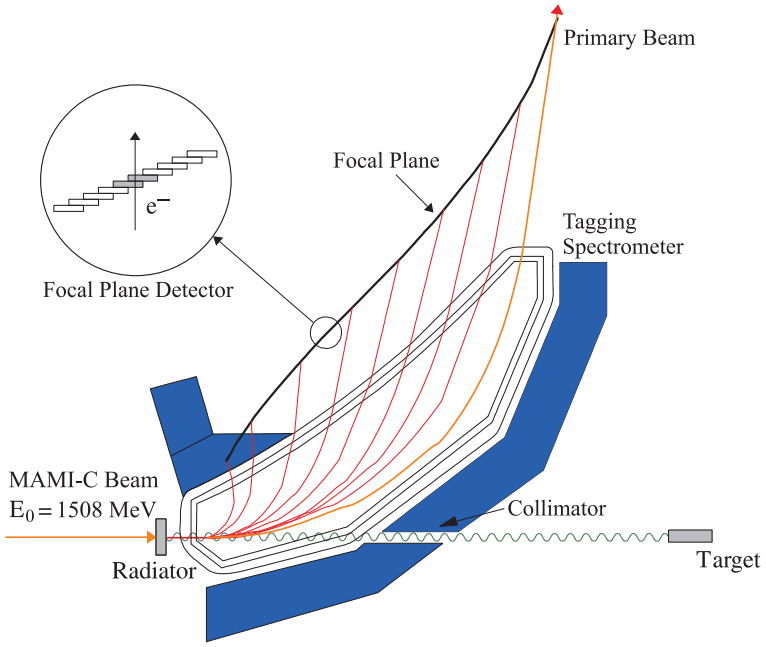

Figure 12: The Glasgow-Edinburgh-Mainz photon tagging spectrometer

A.2 Frozen-spin target

Polarization experiments using high density solid-state targets in combination with tagged photon beams can reach the highest luminosities. For the double polarisation measurements planned with the Crystal Ball detector on polarized protons and deuterons a specially designed, large horizontal ^{3}He/^{4}He dilution refrigerator was built in cooperation with the Joint Institute for Nuclear Research (JINR) Dubna (see Figure 13). It has minimum limitations for the particle detection and fits into the central core of the inner Particle Identification Detector (PID 2). This was achieved by using the frozen spin technique with the new concept of placing a thin superconducting holding coil inside the polarization refrigerator. Longitudinal and transverse polarisations are possible.

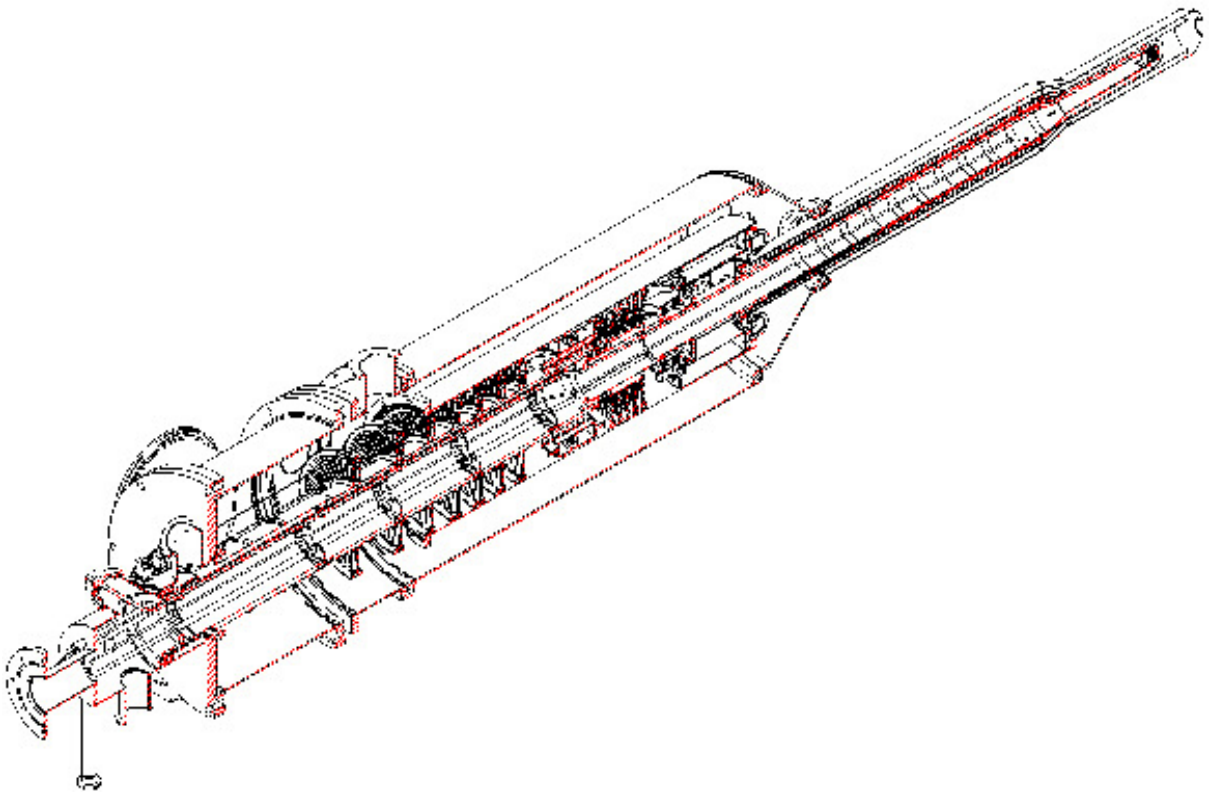

Figure 13: The new dilution refrigerator for the Crystal Ball detector

Highest nucleon polarization in solid-state target materials is obtained by a microwave pumping process, known as dynamic nuclear polarization (DNP). This process is applicable to any nucleus with spin and has already been used in different experiments with polarized proton and deuteron targets. The geometric configuration of the target is the same for the polarized proton and neutron setup. However, since the polarization measurement of the deuteron is more delicate due to the small size of the polarization signals, the modification of some basic components is needed. The reason for this is twofold: firstly the magnetic moment of the deuteron is smaller than that of the proton and, in addition, the interaction of the deuteron quadrupole moment with the electric field gradient in the sample broadens the deuteron polarization signal. An accuracy $\delta P_p/P_p$ of 2 - 3% for the protons and $\delta P_D/P_D$ of 4 - 5% for the deuterons is expected in the polarization measurement. It has also to be taken into account that the measured deuteron

polarization P_D is not equal to the neutron polarization P_n. Assuming a 6 % admixture of the D-state of the deuteron, a calculation based on the Clebsch-Gordon coefficients leads to $P_n = 0.91\ P_D$. Several polarized proton and deuteron materials are available such as alcohols and deuterated alcohols (e.g. butanol $C_4H_{10}O$), NH_3, ND_3 or ^{6}LiD. The most important criteria in the choice of material suitable for particle physics experiments are the degree of polarization P and the ratio K of free polarizable nucleons to the total number of nucleons. Further requirements on polarized target materials are a short polarization build-up time and a simple, reproducible target preparation. The polarization resistance against radiation damage is not an issue for experiments with a low intensity tagged photon beam ($I_\gamma \approx 5 \times 10^7 \gamma$ /sec) as will be used here. However, the limitations of a reduced relaxation time due to overheating of the target beads (Kapitza resistance) will have to be investigated.

Taking all properties together, butanol and deuterated butanol are the best material for this experiment. For protons we expect a maximum polarisation of $P_p = 90$ % and an average polarisation of $P_p = 70$ % in the frozen spin mode. Recently, a deuteron polarization $P_D = 80$ % was obtained with Trityl doped butanol targets at 2.5 T magnetic field in a ^{3}He/^{4}He dilution refrigerator. At a 0.4 T holding field an average neutron polarization P_n (see above) of 50 % will be obtained. The filling factor for the $\approx$ 2mm diameter butanol spheres into the 2cm long, 2cm diameter target container will be around 60 %. The experience from the GDH runs in 1998 [11] shows that, with a total tagged photon flux of 5×10^7, relaxation times of about 200h can be expected. The polarization has to be refreshed by microwave pumping every two days.

In conclusion, we estimate that we will achieve the following target parameters:

- Maximum total tagged photon flux in the energy range of 4 - 95% E_0: $I_\gamma \approx 5 \times 10^7 \gamma sec^{-1}$, with relaxation time of 200 hours.
- Target proton density in 2cm cell: $n_T \approx 9.1 \times 10^{22} cm^{-2}$(including dilution and filling factors)
- Average proton polarisation $P_p = 70$ %
- Target deuteron density in 2cm cell: $n_T \approx 9.4 \times 10^{22} cm^{-2}$(including dilution and filling factors)
- Average neutron polarisation $P_n = 50$ %

A.3 Crystal Ball Detector System

The central detector system consists of the Crystal Ball calorimeter combined with a barrel of scintillation counters for particle identification and two coaxial multiwire proportional counters for charged particle tracking. This central system provides position, energy and timing information for both charged and neutral particles in the region between 21° and 159° in the polar angle, θ, and over almost the full azimuthal (ϕ) range. At forward angles, less than 21°, reaction products are detected in the TAPS forward wall. The full, almost hermetic, detector system is shown schematically in Fig. 14 and the measured two-photon invariant mass spectrum is shown in Fig. 15.

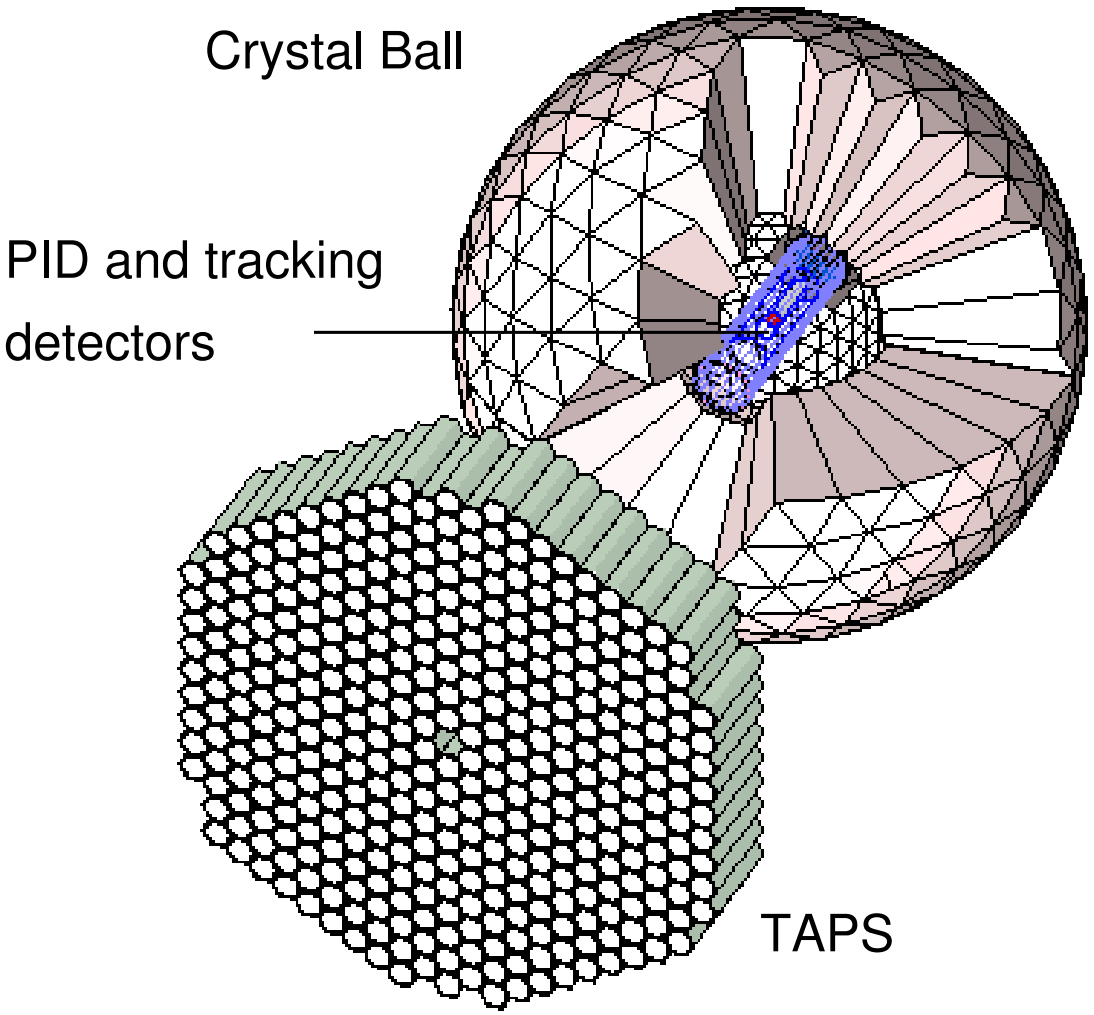

Figure 14: The A2 detector setup: the Crystal Ball calorimeter with cut-away section showing the inner detectors and the TAPS forward wall.

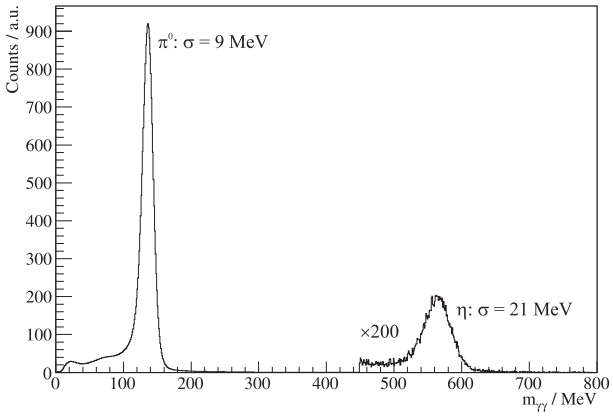

Figure 15: Two gamma invariant mass spectrum for the CB TAPS detector setup. Both η and π^0 mesons can be clearly seen.

The Crystal Ball detector is a highly segmented 672-element NaI(Tl), self triggering photon spectrometer constructed at SLAC in the 1970's. Each element is a truncated triangular pyramid 41 cm (l5.7 radiation lengths) long. The Ball has an energy resolution of $\Delta E/E = 0.020(E[GeV])^{0.36}$, an angular resolution in σ_θ of $2-3^\circ$ and σ_ϕ of $\sigma_\theta/\sin\theta$ for electromagnetic showers [12]. The readout electronics for the Crystal Ball were completely renewed in 2003, and it now is fully equipped with SADCs which allow for the full sampling of pulse-shape element by element. In normal operation, the onboard summing capacity of these ADCs is used to enable dynamic pedestal subtraction and the provision of pedestal, signal and tail values for each element event-by-event. Each CB element is also newly equipped with multi-hit CATCH TDCs. The readout of the CB is effected in such a way as to allow for flexible triggering algorithms. There is an analogue sum of all ADCs, allowing for a total energy trigger, and also an OR of groups of sixteen crystals to allow for a hit-multiplicity second-level trigger - ideal for use when searching for high multiplicity final states.

The excellent CB position resolution for photons stems from the fact that a given photon triggers several crystals and the energy-weighted mean of their positions locates the photon position to better than the crystal pitch. For charged particles which deposit their energy over only one or two crystals, this is not so precise. Here the tracks of charged particles emitted within the angular and momentum acceptance of the CB detector will be reconstructed from the coordinates of point of intersections of the tracks with two coaxial cylindrical multiwire proportional chambers (MWPCs) with cathode strip readout. These MWPCs are similar to those installed inside the CB during the first round of MAMI-B runs [13]. The most significant difference is that all detector signals are taken at the upstream end of the MWPCs, minimising the material required and facilitating particle detection in the forward polar region. A mixture of argon (79.5%), ethane (30%) and freon-CF_4 (0.5%) is used as the filling gas. This mixture is a compromise between charge multiplication and localization requirements imposed by the ionizing particle tracks. Within each chamber both the azimuthal and the longitudinal coordinates of the avalanche will be evaluated form the centroid of the charge distribution induced on the cathode strips. The location of the hit wires(s) will be used to resolve ambiguities

which arise from the fact that each pair of inner and outer strip cross each other twice. The expected angular resolution (rms) will be $\approx 2^\circ$ in the polar emission angle ϑ and $\approx 3^\circ$ in the azimuthal emission angle φ. The MWPCs have been installed inside the CB frame.

The MWPCs provide excellent tracking/resolution information for charged particles. However, in order to distinguish between neutral and charged particles species detected by the Crystal Ball, the system is equipped with PID II, a barrel detector of twenty-four 50 mm long 4 mm thick scintillators, arranged so that each PID II scintillator subtends an angle of 15° in ϕ. By matching a hit in the PID II with a corresponding hit in the CB, it is possible to use the ΔE, E combination to identify the particle species (Fig. 16). This is primarily used for the separation of charged pions, electrons and protons. The PID II covers from 15° to 159° in θ.

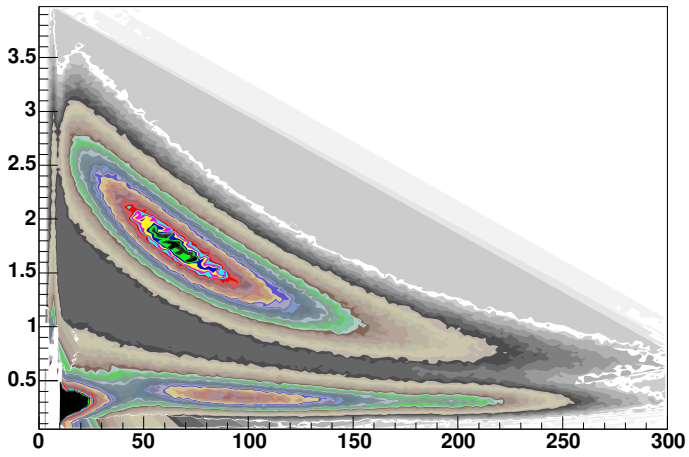

Figure 16: A typical ΔE/E plot from the PID detector. The upper curved region is the proton locus, the lower region contains the pions and the peak towards the origin contains mostly electrons.

A.4 TAPS Forward Wall

The TAPS forward wall is composed of 384 BaF_2 elements, each 25cm in length (12 radiation lengths) and hexagonal in cross section, with a diameter of 59 mm. Every TAPS element is covered by a 5 mm thick plastic veto scintillator. The single counter time resolution is $\sigma_t = 0.2$ ns. The energy resolution can be described by the $\Delta E/E = 0.018 + 0.008/(E[GeV])^{0.5}$ [12]. The angular resolution in the polar angle is better than 1°, and in the azimuthal angle it improves with increasing θ, being always better than 1/R radian, where R is the distance in centimeters from the central point of the TAPS wall surface to the point on the surface where the particle trajectory meets the detector. The TAPS readout was custom built for the beginning of the CB@MAMI program and is effected in such a way as to allow particle identification by Pulse-Shape Analysis (PSA), Time-of-Fight (TOF) and ΔE/E methods (using the energy deposit in the plastic scintillator to give ΔE). TAPS can also contribute to the CB multiplicity trigger and is currrently divided into upto six sectors for this purpose.

References

[1] C. Wu, E. Ambler, R. Hayward, D. Hoppes, and R. P. Hudson, "Experimental test of parity conservation in beta decay," *Phys. Rev.*, vol. 105, p. (1413), 1957.

[2] J. Christenson, J. Cronin, V. Fitch, and R. Turlay, "Evidence for the 2π decay of the k_2^0 meson," *Phys. Rev. Lett.*, vol. 13, 1964.

[3] M. Kobayashi and T. Maskawa, "Cp-violation in the renormalizable theory of weak interaction," *Progress of Theoretical Physics*, vol. 49, p. (652657), 1973.

[4] K. Olive *et al.* (Particle Data Group), "Review of particle physics," *Chin. Phys. C*, vol. 38, 2014.

[5] D. Dicus, "Estimate of the rate of the rare decay $\pi^0 \to 3\gamma$," *Phys. Rev. D*, vol. 12, 1975.

[6] J. McDonough *et al.*, "New searches for the c-noninvariant decay $\pi^0 \to 3\gamma$ and the rare decay $\pi^0 \to 4\gamma$," *Phys. Rev. D*, vol. 38, 1988.

[7] C. Tarbert, "Coherent π^0 photoproduction on nuclei," *Ph.D Thesis - University of Edinburgh*, 2007.

[8] B. K. et al, "Coherent π^0 photoproduction from atomic nuclei," *Phys. Lett. B*, vol. 526, pp. 287–294, 2002.

[9] J. C. M. et al, "Upgrade of the Glasgow photon tagging spectrometer for Mainz MAMI-C," *Eur. Phys. J. A*, 2008.

[10] A. R. et al, "A microscope for the Glasgow photon tagging spectrometer in Mainz," *Eur. Phys. J. A*, 2006.

[11] A. T. et al, "The GDH experiment at MAMI," *Nucl. Phys. B*, vol. 79, p. 591, 1999.

[12] S. P. et al, "Measuremrent of the slope parameter α for the $\eta \to 3\pi^0$ decay with the Crystal Ball dectector at the Mainz Microtron (MAMI-C)," *Phys. Rev. C*, vol. 79, no. 035204, 2009.

[13] G. A. et al, "DAPHNE: a large-acceptance tracking detector for the study of photoreactions at intermediate energies," *Nucl. Instr. Meth. A*, vol. 301, p. 473, 1991.